RESEARCH ARTICLE | SEPTEMBER 05 2025

Experimental aerodynamic analysis of finite flapping wings with chordwise flexibility

Ernesto Sanchez-Laulhe ; Ramon Fernandez-Feria ; Mario Hernandez; Anibal Ollero

Physics of Fluids 37, 091905 (2025)
https://doi.org/10.1063/5.0283561

Physics of Fluids ARTICLE pubs.aip.org/aip/pof

Experimental aerodynamic analysis of finite flapping wings with chordwise flexibility

Cite as: Phys. Fluids **37**, 091905 (2025); doi: 10.1063/5.0283561
Submitted: 2 June 2025 · Accepted: 18 August 2025 ·
Published Online: 5 September 2025

View Online Export Citation CrossMark

Ernesto Sanchez-Laulhe,[1,a)] Ramon Fernandez-Feria,[1] Mario Hernandez,[2] and Anibal Ollero[2]

AFFILIATIONS

[1]Fluid Mechanics Group, University of Malaga, 29071 Málaga, Spain
[2]GRVC Robotics Lab, University of Seville, 41092 Seville, Spain

[a)]Author to whom correspondence should be addressed: ernesto.slaulhe@uma.es

ABSTRACT

Classic two-dimensional aerodynamic results for a heaving and pitching airfoil are normally used for finite flapping wings, taking a reference amplitude at 1/3 of the wingspan from the wingtip. However, for the wings of actual flapping wing robots, flexibility also plays a significant role due to their light weight. For that reason, an analysis of the chordwise stiffness is provided with an experimental testbench, performing low-amplitude pitching motions in the absence of incoming airflow; this allows to obtain the resonance frequency of the structure, enabling the development of an analogy with the theoretical formulation for a deformable heaving airfoil. The beam stiffness term of the airfoil is substituted by that one derived from the resonance frequency. This analogy, which includes the effect of wing inertia through the mass ratio computed from the total mass of the wing, is compared with actual flapping wing experimental results in the wind tunnel. Experiments are performed with two wings of different stiffness characteristics to adequately validate the analysis. Results show excellent agreement with the proposed formulation with similar trends for the evolution of forces at different frequencies and airspeeds. As expected from previous results, the analogy fails when the stiffness term becomes too small ($S < 1$). Results show how the amplitude of the lift oscillations decreases with flexibility, whereas the effects on the average thrust force depend on the reduced frequency, with a critical value around $k \sim 0.6$ beyond which the thrust increases with flexibility.

I. INTRODUCTION

The research interest in flapping wing technology has increased rapidly nowadays, with the development of new aerial robots propelled by this method, looking for safer and more energy efficient designs.[1,2] These flapping wing aerial vehicles (FWAVs) rely solely on their wings to generate the necessary lift and thrust to maintain flight. The development of these aerial platforms has also led to a renewed focus on flapping wing aerodynamics, including the analysis of aeroelastic phenomena.[3–5] Two different cases of flapping wing aerodynamics must be considered, hovering and forward flight. Hovering, which defines the maneuver of flying in a static position, is a typical behavior of insects and small birds. Therefore, FWAVs with hovering capabilities are usually small.[6,7] Larger prototypes[8,9] need to fly forward to obtain the lift force from the incoming aerodynamic velocity, as most birds do. The Strouhal number $St = 2\pi f h_0/U$, which relates the flapping movement (defined by the frequency f and the amplitude h_0) and the forward velocity U, is used to identify the flapping flight case. For hovering, when the Strouhal number is very high ($St \to \infty$), the aerodynamic forces are usually formulated by experimental identification or quasi-steady approximations. On the other hand, aerodynamic forces of the flapping wing in forward flight can be formulated with linear potential theory when the Strouhal number is around 0.3–0.6. This article is focused only on the aerodynamics of flapping wings in forward flight.

The first formulation for the lift force of a heaving and pitching airfoil in forward flight was provided by Theodorsen.[10] The problem was formulated within the linear potential theory framework for a very thin two-dimensional airfoil considering a small amplitude and a harmonic motion. Later, von Kármán and Sears[11] generalized the lift formulation for a heaving and pitching airfoil, although the explicit solution is only provided for the same case of Theodorsen. The thrust of a heaving and pitching airfoil was first formulated by Garrick.[12] The vortical impulse theory, already used by von Kármán and Sears[11] and generalized for an incompressible flow by Wu,[13] was used to improve Garrick's linear inviscid formulation for the thrust force, considering the complete unsteady vorticity distribution on the airfoil.[14] Note that

those results were formulated for a two-dimensional airfoil, not considering the wingspan.

These works were based on a rigid airfoil with prescribed pitching and heaving movements. However, flexibility plays an important role in real prototypes because of the relatively low weight of the wings in FWAVs. Therefore, different formulations have been proposed for the thrust and lift generated by an oscillating airfoil with flexural chordwise deformation. Some works[5,15] consider just a hovering wing, without incoming velocity, which is not the case considered here. The problem has been addressed using numerical[16] and experimental[17] approaches, yielding significant results that facilitate comparison with theoretical models. In the work by Kodali and Kang,[18] Theodorsen formulation is applied for an airfoil with a rigid section around the leading edge and a flexural deformation for the trailing edge. However, their formulation only considers the deformation of the airfoil as a pitching movement, not taking into account the specific pressure distribution. Then, in the work by Du and Wu,[19] the pressure distribution over the deformable airfoil is considered, but the analysis is reduced to a pitching airfoil. With a more general approach, linear potential theory has been used to obtain forces over a heaving and pitching airfoil with a prescribed quadratic deformation.[20] The quadratic deformation serves as a good approximation of the real deformation of a beam up to its first resonance frequency. Then, those results are considered with the beam structural equation, formulating the lift and thrust on a heaving and pitching deformable airfoil.[21] This work showed how passive deformation produces enhancement of the thrust force near the resonance frequency of the airfoil. Propulsion enhancement can also be achieved by active deformation. For instance, by active flexibility with dynamic trailing edge flap, as proposed in Ref. 22. However, active deformation is not considered in this work due to its higher mechanical complexity; so, that case should be addressed in future works.

To go from two-dimensional oscillating airfoils to actual flapping wings, finite wing effects also have to be considered. For that purpose, Theodorsen's formulation was used[23] to model flapping-wing flight, also considering large amplitude wing motion to develop the Modified Strip Theory (MST), based on blade elements. Then, Kim *et al.*[24] further improved this model to include relatively large angles of attack and dynamic stall effects. The blade element method has been used in several works to predict the force of a finite wing, both for hovering[25,26] and for forward flight.[27,28] Recently, it has been used to model bat flight, where wings are highly articulated and have large inertial forces and variable camber, comparing the results with actual flights of these animals.[29] Other works[30,31] have approached the finite wing formulation for pitching wings, obtaining results based on linear potential aerodynamics corrected with the aspect ratio for the definition of forces with different formulations for circulation and added mass effects. For a flapping wing, the common approach is to consider the results of the linear potential theory for a representative amplitude taken at 1/3 of the wingspan.[32]

Those methods approximate the forces on finite flapping wings with results from 2D aerodynamics. However, they do not analyze the 3D flow over the finite wing, and therefore the effects of vorticity in the direction of the chord (e.g., tip vortices) on the flapping wing aerodynamics. Here, we use this approximation to adapt the two-dimensional results of linear potential aerodynamics to finite flapping wings, as done in previous works[33] for rigid wings. However, flapping wings from actual prototypes are normally very lightweight, and therefore the non-dimensional stiffness is reduced, in particular in the chordwise direction. Therefore, flexural effects should also be taken into account. For that purpose, we shall use the results for a heaving and pitching deformable airfoil,[21] adapted for a finite wing.

The main contribution of this article is to provide a comparative analysis between the results of linear potential aerodynamics for an oscillating airfoil and the measured results for a finite flapping wing in wind tunnel experiments. To take into account the flexibility effects, two different wings based on that of the E-Flap prototype[8] are used in the experiments, as these effects are important in the region near the resonance frequency of the wing. To perform the comparison, we use the previously mentioned analogy of the flapping wing as a uniform plunging flat plate with the characteristic amplitude at 1/3 of the wingspan. Then, an analysis of the wing structure is included to estimate the order of magnitude chordwise stiffness of the wing based on its design parameters. The first resonance frequency of the structure is obtained using an experimental testbench designed for this purpose. With the resonance frequency and the mass of the wing, the characteristic parameters used in the theoretical model[21] for the deformable airfoil are identified. Then, the experimental analysis shows the precision of the proposed analogy by comparing the theoretical results with the forces in flapping wings measured in a wind tunnel.

The article is structured as follows. Section II describes the wing, defining its design parameters and structural elements, including a preliminary analysis of the stiffness based on the chordwise structural rods, and an experimental identification of the resonance frequency. Then, the aerodynamic analysis is presented in Sec. III, defining the characteristic parameters needed to develop the aerodynamic analogy, taking into account the chordwise flexural deformation. The formulation of the inertia forces is included in Sec. IV, as they may be important in wind tunnel experiments. The results of the experiments for both wings are presented in Sec. V, including a comparison with the analytical formulation. Finally, some concluding remarks are given in Sec. VI.

II. STRUCTURAL CHARACTERIZATION

The wing is composed of a spanwise carbon fiber bar, five chordwise carbon fiber rods with their five joints 3D printed in PLA (polylactic acid), and the fabric which acts as the aerodynamic surface. The bar is 0.71 m long, with a circular ring section whose outer diameter is 6 mm and inner diameter is 4 mm. This bar is placed at a quarter of the chord from the leading edge for all the wingspan. The hinge provides the rest of the wingspan to the 0.75 m presented in Fig. 1. The rods have a separation of 15 cm. The material and thickness of the rods determine the stiffness of the wing. The aerodynamic surface is made of fabric, attached to the rods with tape, and glued to the end of the spanwise bar. The total surface of the pair of wings is 0.432 m^2, but for the analysis developed here, the surface is reduced to $S_w = 0.20\,m^2$ for a single wing, without the section from the first rod to the flapping axis, which is not strengthened by any element. The schematic design is shown in Fig. 1 with its characteristic measures.

In the original prototype,[8] the diameter of the rods was 1.5 mm. However, the wings were later modified. For example, validation experiments for dynamic models[33] were performed with a wing with 2 mm rods. The flight performance of the prototype with both wings in those past works was similar, and the replacement was mainly due to ensuring the robustness of the wings during a higher number of flights.

The wing weighs 43.2 g in total. The contributions of the four different parts to the total weight are as follows:

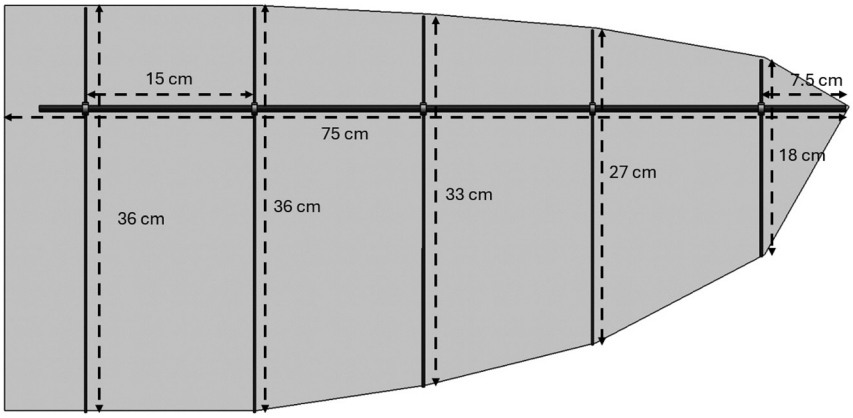

FIG. 1. Schematic design of the wing with measurements for the rods and spanwise bar. Chordwise stiffness is provided by the five rods that hold the fabric.

- Carbon fiber spanwise bar: The density of carbon fiber is measured from an original bar with a length of 2 m, providing a density of $\rho = 1400\,\mathrm{kg/m^3}$. Then, the mass is computed for a bar of 0.72 m, resulting in $m_{bar} = 15.6\,\mathrm{g}$.
- Plastic joining parts: The five pieces weigh 2 g in total, resulting in an individual mass of $m_{JP} = 0.4\,\mathrm{g}$ per part.
- Carbon fiber rods: As with the spanwise bar, the density is measured from an original rod with a length of 2 m, providing a density of $\rho = 1640\,\mathrm{kg/m^3}$. The resulting masses of the five rods are $m_{rod,CF} = [1.85, 1.85, 1.70, 1.39, 0.93]\,\mathrm{g}$, giving a total mass of 7.7 g.
- Fabric: The original surface density of the fabric is $42\,\mathrm{g/m^2}$, leading to a total mass of 8.22 g. However, the weight of the tape and the glue has to be added, resulting in a total mass of $m_S = 17.9\,\mathrm{g}$ for the aerodynamic surface, more than the double of the original density. For computing the inertia, we will consider the mass to be equally distributed on the surface, providing a density of $91.3\,\mathrm{g/m^2}$.

The original design resulted in a rather rigid wing. To analyze the effect of flexibility, experiments were also performed with a more flexible wing, so the differences related to different stiffnesses could be properly identified. For this wing, the chordwise carbon fiber rods with 2 mm diameter were replaced by steel rods with a diameter of 1 mm. Steel is a less rigid material when compared with carbon fiber, with a slightly lower elastic modulus and a higher density, and the diameter of the rods also plays an important role in the wing stiffness, as it will be discussed in Sec. II A. The masses of these five rods are $m_{rod,S} = [2.18, 2.18, 2.00, 1.63, 1.09]\,\mathrm{g}$, giving a total mass of 9.1 g. Therefore, the total mass of the wing increases by 1.4 g.

To characterize the chordwise flexibility of the wing as a function of the material and thickness of the wing rods, a simplified theoretical analysis is performed in Sec. II A for estimating the resonance frequency. Then, an experimental testbench is defined in Sec. II B, providing validation for the estimation and greater precision for the measurement of the resonance frequency.

A. Theoretical analysis of the wing chordwise stiffness

In this section, we provide a theoretical analysis of the resonance frequency of the wing in the chordwise direction. To do so, the characteristics of the specific material and joints have to be considered. The elements along the chord direction are the rods and the fabric, while the PLA joints fix the movement at one quarter length of the chord. The stiffness provided by the fabric is negligible, so the wing chordwise stiffness is completely defined by the five rods distributed along the wingspan. Then, the structural resonance frequency provided by the beam equation is

$$f_{r0} = \frac{1.875^2}{2\pi}\sqrt{\frac{EI}{mL^3}}, \tag{1}$$

with m being the mass and L the length. Note that this length and mass are considered from the joining point, so only the section between the joints and the trailing edge is considered, which is 3/4 of the chord length. Note that the wing can be considered to be clamped at the joints, so the equation for obtaining the resonance frequency has to include only the section from the clamping point, in this case 3/4 of the chord. Then, the stiffness characteristics are given by the elastic modulus E and the second moment of area of the cross section I.

For carbon fiber, the elastic modulus is $E = 220\,\mathrm{GPa}$. For steel, the modulus is similar, around $E = 200\,\mathrm{GPa}$. All the rods have a circular section, so the second moment of area is the same regardless of the direction. It is provided by

$$I = \frac{\pi r^4}{4}, \tag{2}$$

with r the radius of the rod cross section. For the initial carbon fiber rods of diameter 2 mm we have $I \approx 0.79\,\mathrm{mm^4}$, and for the steel rods of diameter 1 mm, $I \approx 0.05\,\mathrm{mm^4}$.

Then, the additional difference in flexibility is provided by the material density: the density of carbon fiber rods is $\rho_{CF} = 1700\,\mathrm{Kg/m^3}$ and the steel density is $\rho_S = 7700\,\mathrm{Kg/m^3}$. The resonance frequency of the isolated rods is given by

$$f_{r0} = \frac{1.875^2 r}{4\pi L^2}\sqrt{\frac{E}{\rho_{CF/S}}}, \tag{3}$$

computing the mass as a function of the density, cross section area, and length, $m = \rho_{CF/S} AL$ with $A = \pi r^2$. By this formula, the resonance frequencies of the carbon fiber rods are $f_{r0,CF} = [44.4, 52.9, 79.0, 177.8]\,\mathrm{Hz}$ for the four lengths (longer to shorter), and those of the steel rods are $f_{r0,S} = [9.8, 11.6, 17.4, 39.1]\,\mathrm{Hz}$. These resonance

frequencies are higher than the usual flapping frequencies of the ornithopter. However, the effect of the fabric must be considered.

As mentioned above, the fabric does not provide any additional stiffness to the wing. However, the added mass of the material substantially modifies the resonance frequency. Note that a higher mass leads to a reduction of the resonance frequency as the inertia of the system increases. Therefore, an estimation of the resonance frequency can be provided considering the sum of the stiffness provided by the five rods,

$$f_{r0} = \frac{1.875^2}{2\pi}\sqrt{\frac{5(EI)_{rod,CF/S}}{\frac{3m_w}{4}\left(\frac{3c}{4}\right)^3}} = \frac{1.875^2}{2\pi}\sqrt{\frac{1080}{81}\frac{(EI)_{rod,CF/S}}{m_w c^3}}, \quad (4)$$

where $3/4$ of the mean chord length are used as reference length and the mass of the wing is comprised of the mass of the fabric and the rods $m_w = (m_S + \sum m_{rod,CF/S})$. This formula provides a resonance frequency of $f_{r0} = 33.9$ Hz for the wing with carbon fiber rods and $f_{r0} = 7.8$ Hz for the wing with steel rods. Although these values may provide a reasonable estimate for the resonance frequency, the real value may differ due to the structural complexity of the system with the combination of different materials and the effects of the fabric. To obtain the actual value analytically, a complex analysis would be required to take into account the influence of all the different parameters, which is not the purpose of this work. For that reason, a testbench is proposed to identify the resonance frequency in the chordwise direction experimentally and evaluate the precision of the estimation in Eq. (4).

B. Experimental identification of the resonance frequency

The purpose of the experiments described here is to identify the structural resonance frequency of the wing in the chordwise direction *in vacuo*. Therefore, identification must be performed without aerodynamic effects, with no inflow velocity, in a specific testbench created for this purpose. Instead of the usual flapping movement, the designed mechanism performs a low-amplitude pitching movement from the span bar. The pitching movement allows an easier identification of the chordwise deformation by recording a video from the wingspan direction [see Fig. 2 (Multimedia view)], at the same time that reduces the forces and spanwise deformation with respect to the flapping movement. Chordwise deformation can be seen in the camber of the wing, easily observed in the rods. Experiments are carried out at different frequencies to look for the maximum deformation of the trailing edge. The design is shown in Fig. 2.

The choice of a continuous rotation motor is optimal for reaching high frequencies over a positioned controlled servomotor. However, a transmission system is needed to transform the rotation of the motor into the desired pitching movement. There are two sections, the gears and the transmission bars, presented in blue and red, respectively, in Fig. 2(a). The motor used for the test bench is an 1130 Kv brushless motor similar to that used in the E-Flap prototype.[8] The gears have 8 and 48 teeth, resulting in a reduction of 6:1. Therefore, the maximum theoretical pitching frequency would be 50 Hz. However, the structural limits of the mechanism provide a lower limit for the frequency. The gears are 3D printed in resin to obtain a higher precision, avoiding transmission loss. The transmission from the second gear to the wing is achieved by a three-bar mechanism. The first bar is in the same gear, where a joint is included at a radius of 5 m from the rotation axis. The second bar then acts as a lever, moving the third bar. This third bar is directly connected to the wing, rotating together.

To perform the analysis, the frequency is increased progressively, and the movement is recorded from an overhead view, to see the deformation of the rods. A support had to be added to avoid movement of the wingtip and spanwise deformation. The testbench is fixed with an aluminum structure attached to a table to avoid additional movement as seen in Fig. 2(b).

The experiments with the wing incorporating carbon fiber rods did not show significant chordwise deformation, even at frequencies higher than 10 Hz. Beyond that frequency, torsional deformations started to appear on the spanwise bar, making the results unreliable. Furthermore, 10 Hz is a significantly higher frequency than the frequencies typically observed during flight. Therefore, the original wing operates far below the resonance frequency during flight, so the aeroelastic effects will be almost negligible. On the other hand, the wing with steel rods showed a different experimental behavior. Chordwise deformation of rods was observed even at low frequencies, around 3 Hz. These results show how this wing can be considered flexible chordwise at normal flight flapping frequencies. The maximum deformation was obtained for 8 Hz, very close to the predicted 7.8 Hz resonance from Sec. II A, showing that the theoretical estimation proposed is precise enough in this case, so no further structural analysis is esteemed necessary.

The resonance frequency of the wing will serve to define the characteristic stiffness in Sec. III with the theoretical aeroelastic formulation for an airfoil.[21] For the wing with steel rods, we shall use the experimentally identified frequency, while for the wing with carbon fiber rods the theoretical value computed in Sec. II A will be used instead.

III. THEORETICAL AEROELASTIC ANALYSIS

The aerodynamic formulation of a pitching and heaving airfoil including chordwise deformation was obtained for a prescribed deformation.[20] Later, the deformation was obtained through the beam bending equation, thus presenting the performance of an airfoil with passive flexibility.[21] In these works, the proposed chordwise deformation is modeled by quadratic and quartic flexural deformations. This type of deformation is the one obtained in the experiments in Sec. II B, and produces passive changes in the wing camber. We take this formulation for the aeroelastic analysis, considering just the heaving motion. However, we need to go from the aerodynamic formulation of a flexible heaving airfoil to an actual flapping wing like the one used here. This section proposes an analogy to define the characteristic parameters used for the airfoil formulation in our finite flapping wing. The analogy does not consider the effects of 3D deformations and vorticity over the wing, but just intends to serve as an approximation for applying known results from 2D linear potential aerodynamics to finite flapping wing, as done in previous works for rigid wings.[32,33]

The first aspect to consider is that the amplitude of the flapping motion varies along the wingspan. If the formulation is developed with the results of previous works, a reference amplitude is needed. Therefore, we take this reference amplitude at $1/3$ the wingspan from the wingtip, as done in previous works.[33] Then, the dimensionless amplitude is given by

$$h_0 = \frac{b}{3c}\sin(\phi), \quad (5)$$

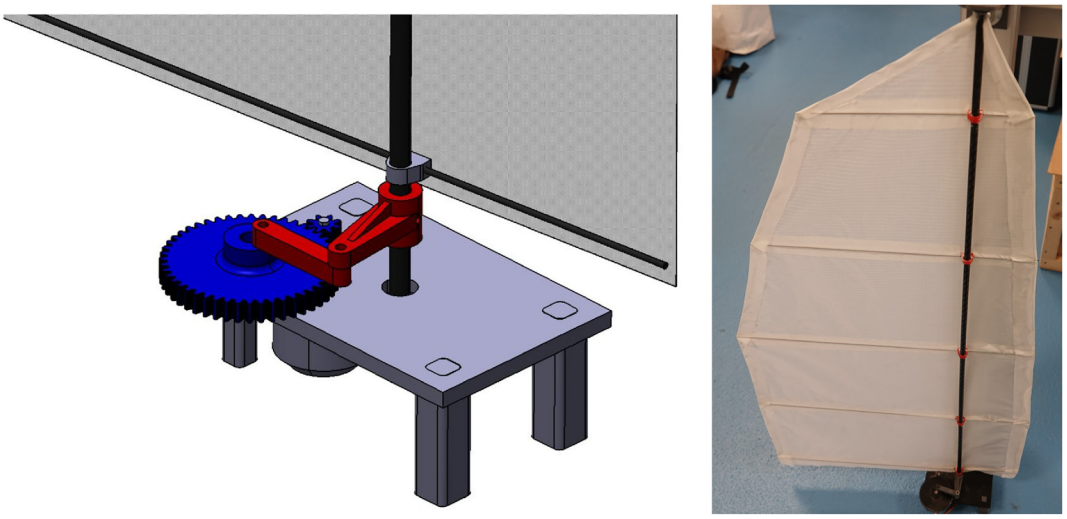

(a) CAD design. In blue the reduction gears and in red the transmission mechanism of the test bench for the resonance frequency.

(b) Image of the testbench with the wing fixed to an aluminum structure to avoid vibrations.

FIG. 2. Experimental testbench for the resonance frequency. Multimedia available online.

with ϕ being the angular amplitude of the flapping movement, b the wingspan of the ornithopter, and c the mean chord. The reduced dimensionless frequency is defined as[21]

$$k = \frac{\omega c}{2U}, \tag{6}$$

with $\omega = 2\pi f$ the angular flapping frequency and U the airspeed. The reduced frequency and flapping amplitude are the two parameters that define the flapping motion.

Then, to analyze the structural deformation of the airfoil as a beam, the two ruling parameters are the mass ratio R and the dimensionless stiffness S provided in previous works[21] as follows:

$$R(x) = \frac{\rho_s(x)\varepsilon(x)}{\rho c}, \quad S(x) = \frac{E(x)\varepsilon^3(x)}{\rho U^2 c^3}, \tag{7}$$

where ρ_s and ρ are the densities of both the airfoil and the air, and ε is the thickness of the airfoil. As also done in previous works,[21] we consider the density, the elastic modulus, and the thickness to be constant along the chord, since both the rods and the fabric have constant density and thickness, and the elastic modulus should also be constant. This approximation was also made in Sec. II A to estimate the resonance frequency of the structure. For the finite flapping wing, the mass ratio can be computed with the mass of the wing,

$$R = \frac{m_w}{\rho S_w c}. \tag{8}$$

However, dimensionless stiffness includes the velocity, which is modified in each experiment. Therefore, the analogous parameter to be determined is the term $E\varepsilon^3/c^3$. To that end, the resonance frequencies experimentally identified in Sec. II B will be used to obtain the stiffness. The reduced resonance frequency *in vacuo* of an airfoil was obtained in Ref. 21 as

$$k_{r0} = \sqrt{F(a)}\sqrt{\frac{S}{R}} = \sqrt{\frac{280(1+3a^2)}{141+168a+1281a^2-1120a^3+1015a^4+315a^6}\frac{S}{R}}, \tag{9}$$

where a is the non-dimensional pivot point of the airfoil, in which the airfoil is fixed to the prescribed flapping movement. Note that the function of the pivot point $F(a)$ can be considered constant in our case, since the pivot point is fixed in $c/4$, where $a = -0.5$. If the dimensional terms are included, from Eqs. (6)–(9), we have

$$\frac{\pi f_{r0} c}{U} = \sqrt{F(a)}\sqrt{\frac{E\varepsilon^3 S_w}{m_w U^2 c^2}}, \tag{10}$$

and the term for the analogous stiffness can be isolated,

$$\frac{E\varepsilon^3}{c^3} = \frac{\pi^2 f_{r0}^2 m_w c}{S_w F(a)}. \tag{11}$$

This equation directly relates the stiffness term with the resonance frequency. For the wing with steel rods, using the identified frequency in Sec. II B, we obtain $E\varepsilon^3/c^3 = 31.6$ Pa. Meanwhile, for the wing with carbon fiber rods this term is computed with the estimated frequency of Sec. II A, obtaining $E\varepsilon^3/c^3 = 536.8$ Pa.

With this novel analogy proposed, the characteristic parameters of the wing are obtained. Then, we apply the previous formulation for

a heaving airfoil.[20,21] This formulation is written here explicitly as it is used for the comparison between theoretical and numerical results in Sec. V. The amplitude and the reduced frequency define the flapping movement,

$$h(t) = \Re\left[h_0 e^{ikt}\right]. \tag{12}$$

Then, the flexural quartic approximation of the deflection is defined with the same frequency and a certain phase shift ψ_d,

$$d(t) = \Re\left[d_m e^{i\psi_d} e^{ikt}\right]. \tag{13}$$

Note that, as commented in previous works,[21] the quartic approximation is the minimal model that allows the beam equations to be applied for the chordwise deformation. Furthermore, the approximation works quite accurately for the first natural frequency of the system. However, both the amplitude d_m and the phase ψ_d of the deflection are unknown. Those terms were obtained in Ref. 21 for a harmonic motion,

$$d_m = \left|\frac{F_1(R,k,h_0,a)}{F_2(R,S,k,a)}\right|, \quad \psi_d = arg\left(\frac{F_1(R,k,h_0,a)}{F_2(R,S,k,a)}\right), \tag{14}$$

where the complex functions F_1 and F_2 are

$$F_1 = -h_0 k^2\left[4R\left(a^2+\frac{1}{3}\right)+\pi\left(a^2+\frac{1}{4}\right)\right]+2\pi(a^2+a+1)\mathscr{C}(k)ikh_0, \tag{15}$$

$$\begin{aligned}F_2 = {} & 4Rs_f(a)k^2-\frac{16}{3}\left(a^2+\frac{1}{3}\right)\frac{S}{(1-a)^2}+\frac{\pi a}{4}\left(Bk^2+2Dik+\frac{Ek^2}{2}+2Jik\right)\\ & +\frac{\pi a}{2}(Dik-3E+Jik)+\frac{\pi}{4}\left(3a+\frac{1}{2}\right)(-Eik+4J)+\pi\left(a^2+\frac{1}{4}\right)\\ & \times(Ak^2+Bik)+\frac{\pi}{4}\left(a^2+\frac{1}{3}\right)(Dk^2+3Eik)+\pi\left(a+\frac{1}{4}\right)(2D-Bik)\\ & +\pi\left(a^2+\frac{3}{8}\right)\frac{Jk^2}{8}-\pi\left(a^2+a+\frac{1}{2}\right)\mathscr{C}(k)\left\{(2A-B+D)ik\right.\\ & \left.-2B+2D-3E+\frac{3}{4}[(J-E)ik+4J]\right\},\end{aligned} \tag{16}$$

with the functions of the pivot point[21] $s_f(a)$, A, B, D, E and J, and the Theodorsen's function $C(k)$[10] are provided in Appendix A. Note that, as described in Ref. 21, the resonance frequency considering the fluid–structure interaction is obtained by minimizing the function F_2.

Once the deflection amplitude and phase are defined, we can formulate the lift and the thrust. For simplicity, here an updated formulation[34] is used instead of the first preliminary results for a deformable airfoil.[20] The lift coefficient is given by

$$C_{L,a}(t) = \pi[-\ddot{h} + A_{l2}(a)\ddot{d} + A_{l1}(a)\dot{d}] + \mathscr{C}(k)\Gamma_0(t), \tag{17}$$

where the quasi-steady circulation is

$$\Gamma_0(t) = -2\pi[\dot{h} + A_{g1}(a)\dot{d} + A_{g0}(a)d], \tag{18}$$

and the four functions of the pivot point[34] A_{l2}, A_{l1}, A_{g1}, and A_{g0} are provided in Appendix A for easy reference. For the thrust, just the mean term is computed, given by

$$\bar{C}_T = t_h(kh_0)^2 + t_{hd}kh_0 d_m + t_d d_m^2, \tag{19}$$

where the functions t_h, t_{hd}, and t_d, provided in previous works,[20,21] are also reproduced in Appendix A. The results of these analytical equations, which have been validated against high fidelity numerical simulations,[35] are compared with the experimental results of the forces generated in a wind tunnel in Sec. V.

IV. INERTIA FORCES DURING FLAPPING MOVEMENT

During the flapping movement, additional forces appear in the wing due to its inertia. Those forces have to be considered for the experimental validation as they may significantly affect the results. This section approaches the inertia forces in the wing, considering the spanwise mass distribution.

The coordinates over the wing are provided by the following position vector:

$$\vec{X} = x\vec{e}_x + r\sin(\phi)\vec{e}_y + r\cos(\phi)\vec{e}_z. \tag{20}$$

Note that x corresponds to the chordwise variable of the wing and r to the spanwise variable, as shown in Fig. 3. ϕ is the flapping angle, provided by the known movement of the wing. The second derivative (acceleration) of this function is given by

$$\frac{d^2\vec{X}}{dt^2} = r[\ddot{\phi}\cos(\phi) - \dot{\phi}^2\sin(\phi)]\vec{e}_y - r[\ddot{\phi}\sin(\phi) - \dot{\phi}^2\cos(\phi)]\vec{e}_z. \tag{21}$$

As expected, the acceleration does not include any term in the chordwise direction, affecting only to the lift forces, not to the thrust. The

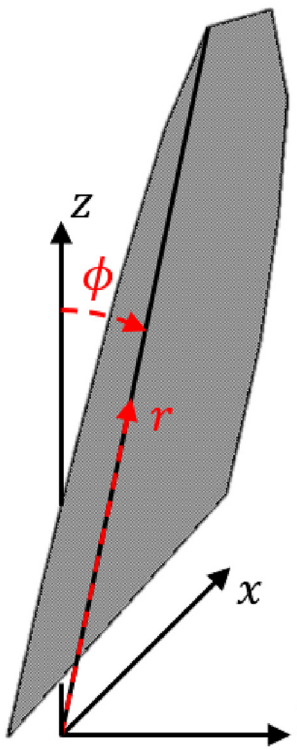

FIG. 3. Coordinates used for inertia computation.

inertia force is provided by the integral of the acceleration and the mass for the entire wing,

$$\vec{F}_R = \int_{r_1}^{r_2}\int_{x_l(r)}^{x_t(r)} \rho_s(r,x)\varepsilon(r,x)\frac{d^2\vec{X}}{dt^2}\,dx\,dr. \tag{22}$$

We can include here Eq. (21) and consider only the lift term, as the forces in the other direction do not affect the aerodynamics,

$$L_R = \vec{F}_R \cdot \vec{e}_y = [\ddot{\phi}\cos(\phi) - \dot{\phi}^2\sin(\phi)]\int_{r_1}^{r_2} r\int_{x_l(r)}^{x_t(r)} \rho_s(r,x)\varepsilon(r,x)dx\,dr, \tag{23}$$

where the integral term defines the center of inertial lift r_0 as

$$r_0 = \frac{\int_{r_1}^{r_2} r\int_{x_l(r)}^{x_t(r)} \rho_s(r,x)\varepsilon(r,x)dx\,dr}{m_{w,s}}, \tag{24}$$

considering the mass distribution of the wing on the surface. Note that this mass term $m_{w,s}$ includes all the masses of the different elements of the wing defined in Sec. II, not only the fabric and the rods as in Eqs. (4) and (8). $r_1 = 7.5$ cm and $r_2 = 75$ cm are the initial and final points of the wingspan from the flapping axis, and x_l and x_t are the leading and trailing edge chordwise coordinates.

The mass parameter includes contributions from four parts, as commented in Sec. II. The plastic pieces and the rods can be included as five point masses along the wingspan, computed as

$$(r_0 m)_p = \sum_{i=1}^{5} r_i(m_{rod,i} + m_{JP}), \tag{25}$$

where the positions of the rods are $[7.5\ 22.5\ 37.5\ 52.5\ 67.5]$ cm, as shown in Fig. 1, and the masses of the rods and the joining parts are provided in Sec. II for both wings. Note that the specific centers of inertial lift are calculated together with the mass for each element to simplify the formulation. The results of the punctual mass parameter for both wings are $(r_0 m)_{p,CF} = 3.3$ g m and $(r_0 m)_{p,S} = 3.7$ g m.

The distributed mass parameter is expressed then as

$$(r_0 m)_d = \int_{r_1}^{r_2}\left(r\frac{m_{bar}}{r_2 - r_1} + r\int_{x_l(r)}^{x_t(r)}\frac{m_S}{S}dx\right)dr. \tag{26}$$

This distributed mass parameter is the same for both wings, as the bar and the surface masses do not change. In this case, this mass term is more significant, with its value $(r_0 m)_d = 12.4$ g m.

Note that the inertia moment has not been considered, as the results of the experiments are focused on the lift and thrust forces, not computing the aerodynamic moment.

V. EXPERIMENTAL VALIDATION

The experiments are carried out with both wings in the wind tunnel at the aero-hydrodynamics laboratory of the University of Malaga (a description of the wind tunnel characteristics and the force and torque sensor can be found in Ref. 36). This section describes the experimental details and the results obtained.

A. Experimental setup

To analyze the forces acting on the flapping wing, an experimental setup was designed for use inside the wind tunnel. The flapping mechanism [see Fig. 4 (Multimedia view)] is similar to that of the E-Flap prototype.[8] However, some changes are made to obtain more accurate results. Instead of the carbon fiber plates that composed the body of the ornithopter, we use aluminum plates with a thickness of 3 cm. This modification is made to avoid flexural deformations in the plates during the flapping oscillations thanks to the increased thickness, considering also that the weight is less restricted than in the ornithopter. The structure is shown in Fig. 4. Gears, motor and electronic speed controller (ESC) are the same as in the original prototype,[8] with a reduction of 42:1. The crank is selected for a flapping amplitude of 15°, which corresponds to a dimensionless amplitude of $h_0 = 0.43$. Note that this amplitude is relatively high but within the limits for which the unsteady aerodynamic forces from the linear potential flow theory for a rigid foil have been validated.[37–39]

The flapping structure is fixed in a force and torque sensor with 6 degrees of freedom, placed parallel to the floor of the wind tunnel, in a circular hole. The structure that holds the sensor is fixed to the wind tunnel structure and the floor to eliminate any possible vibrations. Force measurements are transmitted to the wind tunnel control computer and stored to be post-processed later. The flapping motor is controlled by an RC transmitter. The experiments are performed with a fixed control signal for 10 s, after having previously left a certain time for the stabilization of the system. The four possible control signals

FIG. 4. Flapping mechanism fixed in the wind tunnel. Multimedia available online.

correspond approximately to 1.1, 2.3, 3.4, and 4 Hz, although the exact values may vary due to battery discharge.

In addition, an ELP high-speed USB camera is placed above the wind tunnel to capture top-view recordings of the experiments. The videos are processed by a Python script from the wind tunnel control computer simultaneously with the force measurements from the experiments. The simultaneous recording allows comparing the forces during the flapping cycle by knowing the position of the wing relative to the measurements.

B. Aerodynamic characterization

The experiments are performed with both wings: with carbon fiber rods and with steel rods. Their characteristic parameters are summarized in Table I, where the air density used is $\rho = 1.225\,\mathrm{kg/m^3}$. The mass terms are very similar for both wings. However, the stiffness term $E\varepsilon^3/c^3$ is more than ten times higher for the wing with carbon fiber rods. The center of inertial lift is in a similar position for both wings.

The dimensionless chordwise stiffness S is not included in Table I as it varies with velocity. This parameter is shown in Fig. 5 for both wings. The trend is the same for both cases, decaying as U^2 according to Eq. (7). Note that S is about ten times higher for the wing with carbon fiber rods in Fig. 5(a). The wing with steel rods has a reduced stiffness that becomes of order unit for an airspeed around 5 m/s, as seen in Fig. 5(b), which is the limit for the present aerodynamic analysis.[21]

Due to the different stiffness values, the aerodynamic resonance frequency curve with the velocity has a different shape for both wings, as seen in Fig. 6. The resonance frequency is obtained as defined in previous works,[21] minimizing F_2 [defined in Eq. (16)] as a function of the reduced frequency. We see in Fig. 6(a) how the range of the resonance frequency for the wing with carbon fiber rods is much higher than the normal flight frequencies for the range of flight velocities of the ornithopter (2–6 Hz). On the other hand, for the wing with steel rods, the resonance frequency takes values in the actual flight range, as shown in Fig. 6(b).

TABLE I. Characteristic parameters of both wings.

Rods	f_{r0}	m_w (g)	R	$E\varepsilon^3/c^3$ (Pa)	r_0 (cm)
CF	33.9	25.6	0.35	536.8	36.3
Steel	8	27.0	0.37	31.6	36.1

Two different sets of results are analyzed as functions of the frequency, velocity, and stiffness: the amplitude of the oscillations in the lift coefficients C_{LA} and the mean thrust coefficient $\bar{C}_T$. Logarithmic scale is used for the representation of forces due to the exponential nature of the results with reduced frequency, which leads to a best comparison of the trend of the experiments compared to the analytical solution. Therefore, errors at high reduced frequencies may seem smaller than their real value. In this case, the comparison is more focused on the trend for both analytical and experimental results. The experimental results are compared with the analytical expressions Eqs. (17) and (19), respectively. Note that the mean lift coefficient is zero, according to the unsteady aerodynamic formulation, if the mean angle of attack is also zero. The oscillations in the thrust force are harder to measure precisely because of the added effect of the drag forces.

The analytical results corresponding to both wings are first analyzed in Figs. 7 and 8. The amplitude of the lift coefficient for the wing with carbon fiber rods is very similar to that of a rigid wing. The chordwise flexibility causes the amplitude of the oscillation to decrease, this effect being more important as the velocity increases, but for this wing the effect is almost unnoticeable. We see in Fig. 7(a) how the different curves are almost identical. Then, for the thrust, the effect is important for $k > 1$, for which flexibility provides an increase, as observed in Fig. 7(b), although those frequencies are difficult to reach in actual flights. There is a critical frequency, around $k = 0.65$, under which the flexibility reduces the thrust, although this effect is very small for this wing. Above that frequency, the thrust increases with flexibility. The constancy of this threshold frequency, above which the thrust of the flexible airfoil is larger than that of the rigid airfoil counterpart, for a wide range of stiffnesses was already observed in the analysis of Ref. 21, being related to the approach to the first resonance frequency of the flexible airfoil.

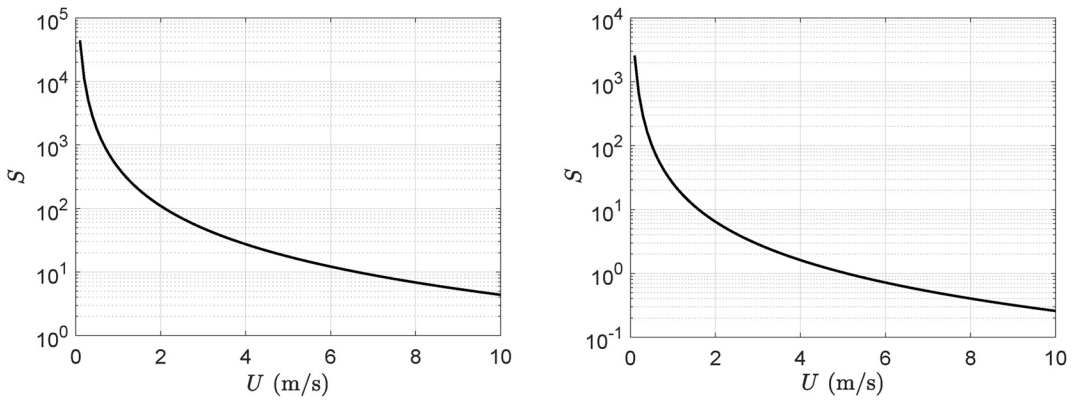

(a) Wing with CF rods. (b) Wing with steel rods.

FIG. 5. Non-dimensional chordwise stiffness of the wing as a function of airspeed. The stiffness parameter decreases with the velocity. For the wing with steel rods, S becomes smaller than 1 at around 5 m/s.

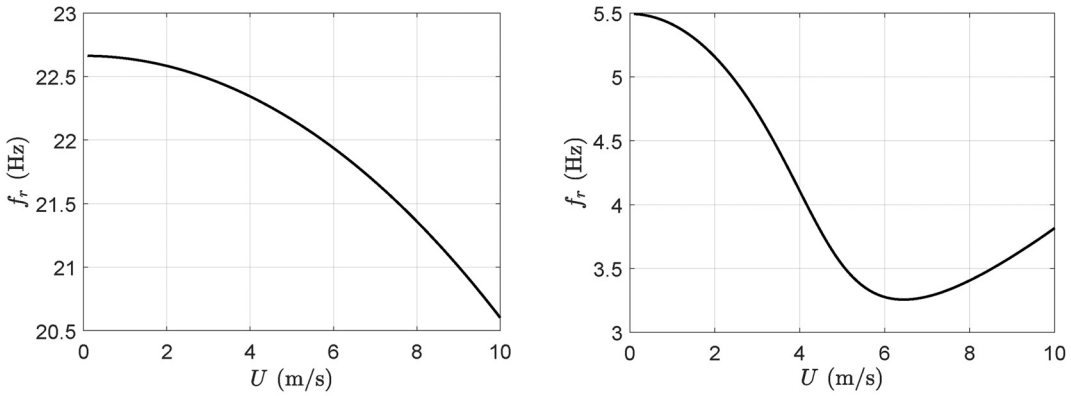

(a) Wing with CF rods. (b) Wing with steel rods.

FIG. 6. Resonance frequency as a function of the airspeed for the characteristics of wings defined in Table I. The minimum value for the wing with steel rods is reached when $S < 1$.

Figure 8 shows the analytical forces for the wing with steel rods. The flexibility effects are more visible here, since the stiffness is lower. Note in Fig. 8(a) how the amplitude of the lift coefficient oscillations decreases with the velocity, as the flexibility effects become greater, due to the passive changes in the wing camber. For $U = 6$ m/s there is a critical point where the first resonance is reached and the oscillations increase. See also in Fig. 8(b) how the behavior for the thrust coefficient is qualitatively the same as commented for the other wing, with a region where flexibility reduces the mean thrust. The critical k from which the thrust increases with flexibility is slightly modified with the velocity, but is still around $k = 0.6$. However, another aspect that we can see here is that, over certain frequencies, the wing is too flexible and the thrust becomes higher for lower velocities, for which the flexibility effect is smaller.

C. Experimental results

The experiments are performed for three wind tunnel operating conditions. The first provides an airspeed around 2 m/s, the second around 3 m/s, and the third around 6 m/s. The airspeed is affected by the wing movement, slightly increasing with the flapping frequency. For that reason, the velocity is measured for all the experiments independently. As commented on before, the frequencies of the experiments are approximately 1.1, 2.3, 3.4, and 4 Hz, but they are also measured accurately for all the experiments. Additionally, the temperature is also measured in all the experiments, providing the density and viscosity of the air, as well as the Reynolds and Strouhal number, given by

$$St = kh_0 = \frac{\pi f c h_0}{U}, \quad Re = \frac{Uc}{\nu}, \tag{27}$$

where ν is the kinematic viscosity.

An example of the outcome of the experimental force measurement can be seen in Fig. 9. Note how the thrust force oscillates with a higher frequency, exactly double, as predicted by the unsteady aerodynamic analysis.[14] This experiment was carried out with the third operative condition of the wind tunnel and the maximum value of the flapping frequency. The lift coefficient is centered at zero and the mean thrust has a positive value. The friction drag, obtained with the

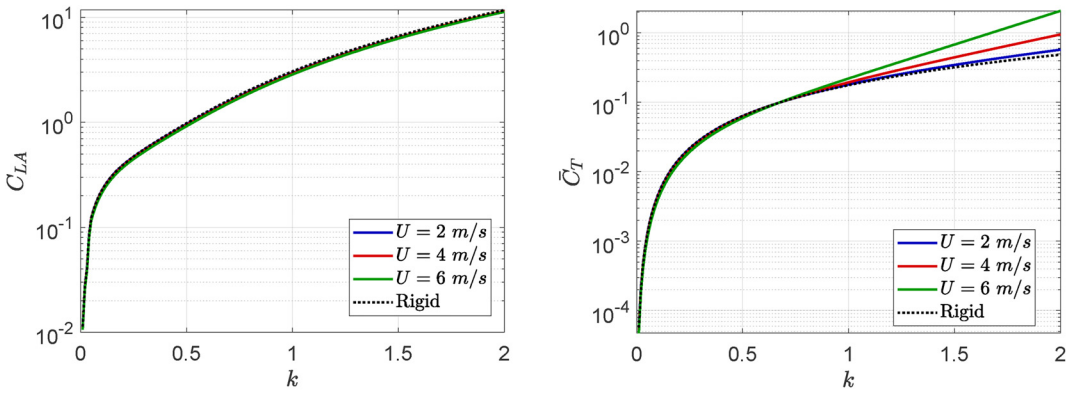

(a) Amplitude of the lift force. (b) Mean thrust coefficient.

FIG. 7. Analytical results for the wing with carbon fiber rods. The flexibility effects are almost negligible, except for the thrust at high reduced frequencies.

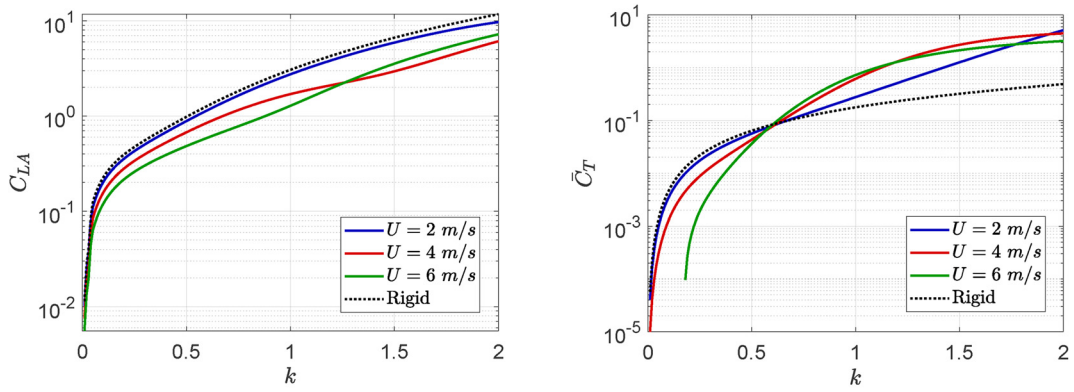

(a) Amplitude of the lift force. (b) Mean thrust coefficient.

FIG. 8. Analytical results for the wing with steel rods. Flexibility effects at different velocities are significant compared to Fig. 7.

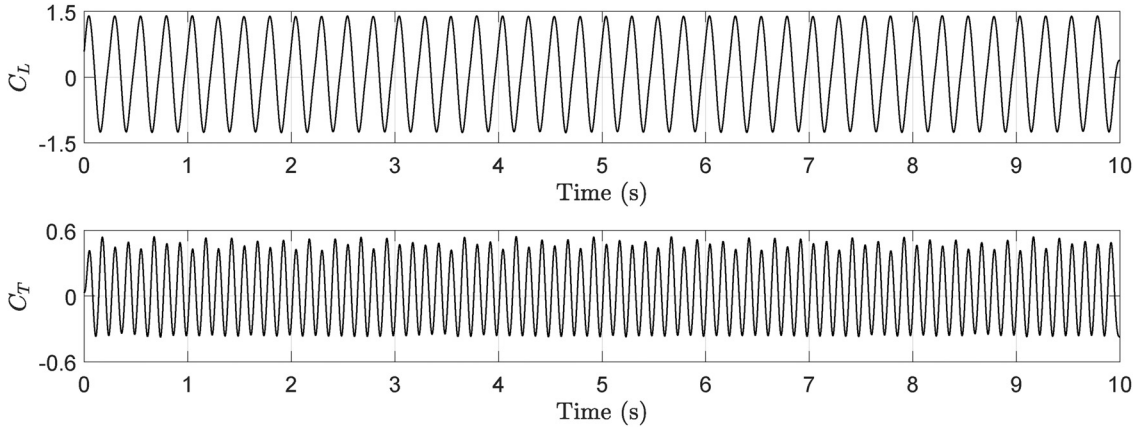

FIG. 9. Experimental results for the lift and thrust coefficient ($f = 4$ Hz, $U = 6.1$ m/s, $k = 0.62$, $S = 12.26$, $Re = 1.13 \times 10^5$). Inertial forces are not subtracted.

static wing, has to be subtracted from the thrust coefficient value to compare with the aerodynamic thrust given by the potential theory.

The temporal evolution of the lift obtained experimentally is compared with the analytical curve in Fig. 10. To do so, both the aerodynamics from Sec. III and the inertia from Sec. IV are considered,

$$C_L = C_{L,a} - C_{L,R}. \tag{28}$$

Inertia is subtracted as the reaction force opposes movement, as it has been formulated in Sec. IV. The coefficients are calculated with Eqs. (17) and (23) respectively, the last one in non-dimensional form dividing by $\frac{1}{2}\rho S U^2$.

Note the strong agreement between the theoretical and analytical results presented in Fig. 10. Both the amplitude and the phase show good alignment. However, the experimental result for the lift coefficient is not exactly sinusoidal. There are several possible explanations for this asymmetry. For example, the transmission mechanism does not generate an exact sinusoidal movement. Furthermore, the wing surface is not continuous as the span bar, as well as the joining parts and the rods, is on the downside of the wing, perturbing the flow.

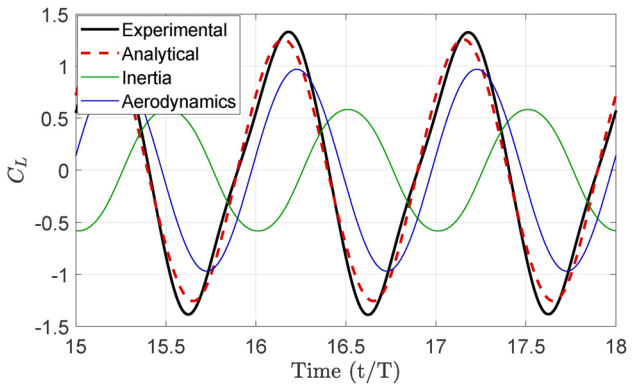

FIG. 10. Comparison between analytical and experimental results for the temporal evolution of the lift coefficient ($f = 4$ Hz, $U = 6.1$ m/s, $k = 0.62$, $S = 12.26$, $Re = 1.13 \times 10^5$). Contributions from aerodynamics and inertia are considered in the analytical solution. Non-dimensional time scaled with the flapping period is used.

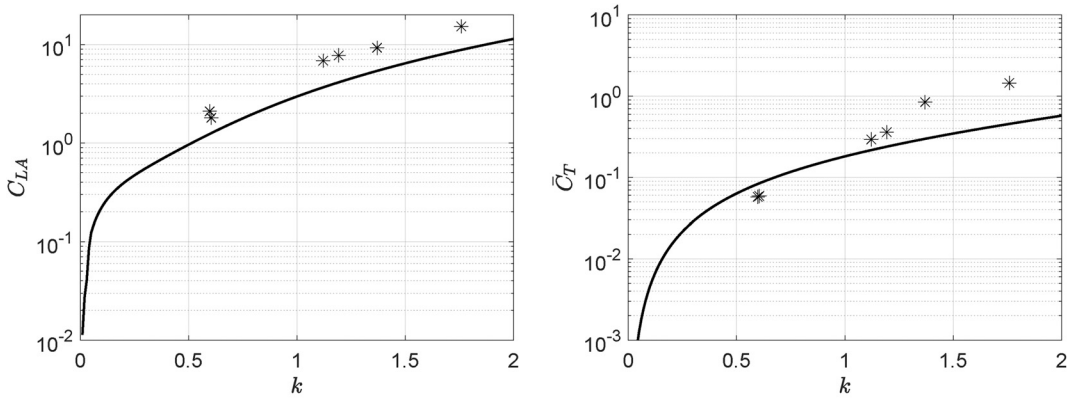

(a) Amplitude of the lift force. (b) Mean thrust coefficient.

FIG. 11. Comparison of the experimental results for the wing with carbon fiber rods (stars) and the theoretical curves at the first operating condition of the wind tunnel ($U \approx 2$ m/s).

Additionally, wing manufacturing process is manual, which introduces uncertainty in its behavior.

A total of 41 experiments were performed with the two wings for different velocities and frequencies. All the characteristics and main results of each experiment are listed in Tables II and III in Appendix B. For the wing with carbon fiber rods, experiments 1–6 are performed at the first operating condition of the wind tunnel, 7–13 at the second condition, and 14–21 at the third condition. As the performance is expected to change with velocity, the experiments are compared with the corresponding theoretical curve separately for clarity.

Figure 11 shows the results for the experiment with the lower velocity. The results are close to the reference analytical curve but with slight differences. For the lift oscillations, the analytical prediction underestimates the lift amplitude. The relatively high heaving amplitude ($h_0 > 0.3$) and a certain spanwise flexibility may explain this small difference. Then, the thrust results are lower than the analytical prediction under the critical frequency and higher for higher frequencies, in a similar way as if the flexibility effects were higher than originally predicted. The increase in lift forces may generate an additional flexural effect, leading to this behavior. However, other aspects such as nonlinear effects due to the relatively high Strouhal number (see St experimental values in Appendix B) may also affect the results at high reduced frequencies, as the 2D linearized theory for a rigid airfoil underpredicts the thrust and lift when the Strouhal number is not small enough,[39] in particular for the more rigid wing with carbon fiber rods.

The agreement is better as the velocity increases. Figure 12 shows the forces for the second operating condition. See in Fig. 12(a) how the experimental results for the lift amplitude are again slightly higher, but the values are near the analytical prediction following a similar trend. The agreement is better at low flapping frequencies for both the lift and the thrust, when the Strouhal number is lower, $St < 0.5$. Again, beyond the critical value of k, the wing acts as if it were more flexible than predicted, producing a higher thrust, the same effect as in Fig. 11(b).

For the third operating condition, the velocity is significantly higher, between 5 and 6 m/s approximately (see Table II). The lift amplitude is accurately estimated with the theoretical values, as shown

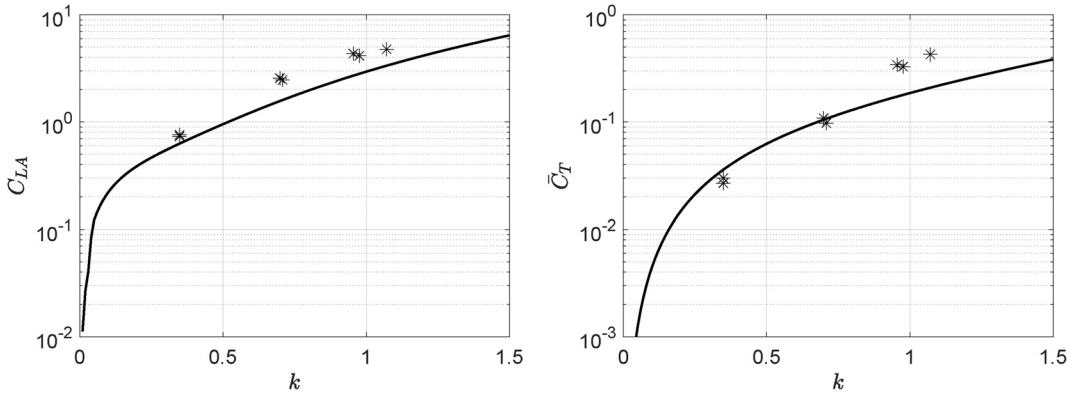

(a) Amplitude of the lift force. (b) Mean thrust coefficient.

FIG. 12. Comparison of the experimental results for the wing with carbon fiber rods (stars) and the theoretical curves at the second operating condition of the wind tunnel ($U \approx 3$ m/s).

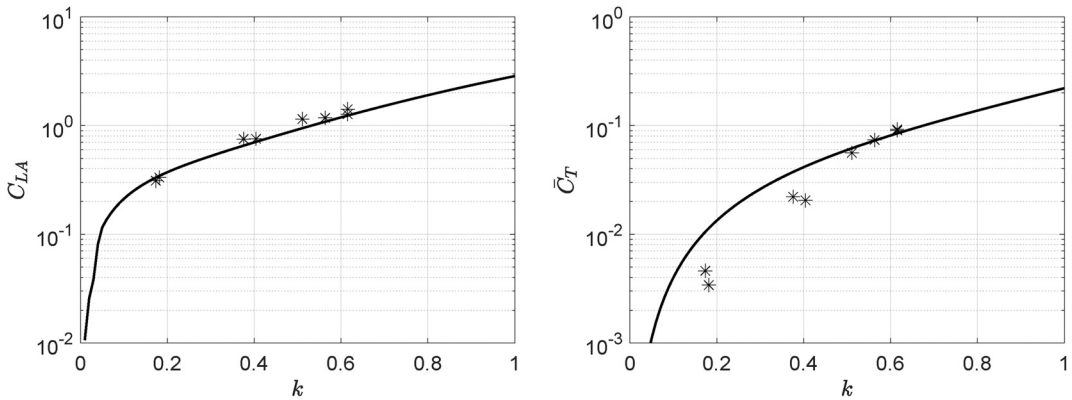

(a) Amplitude of the lift force. (b) Mean thrust coefficient.

FIG. 13. Comparison of the experimental results for the wing with carbon fiber rods (stars) and the theoretical curves at the third operating condition of the wind tunnel ($U \approx 6$ m/s).

in Fig. 13(a). For the thrust, in Fig. 13(b), the estimate is also quite accurate. The logarithmic scale exaggerates the error for the results at low frequencies, which is around $\Delta C_T \sim 0.005$. However, the results around the critical k are almost identical.

In general, these results showed a rather rigid behavior of the wing with a slight underestimate of the lift amplitude and the flexibility effects on the thrust. Results for the wing with steel rods are expected to show a different behavior according to an increased flexibility (see Fig. 8), with a reduction of the lift amplitude for all the cases, while the thrust will depend on the frequency. For this wing, experiments 1–6 have been carried out with the first operating condition of the wind tunnel, 7–12 with the second, and 13–20 with the third (see Table III in Appendix B).

Figure 14 shows the results of the experiments at the lower velocity. As observed with the wing incorporating carbon fiber rods, the lift oscillations have a larger amplitude than predicted. However, the flexibility effect can be seen at higher frequencies, as the experiments follow the decrease in the slope for the lift amplitude predicted by the theoretical curve. The thrust estimation is very precise for this wing, even at higher frequencies. Very similar results are obtained for the second operative condition (Fig. 15). Again, the lift oscillations are slightly underestimated, but the behavior is similar, and the thrust force is accurately estimated for all the range of frequencies.

However, the analytical curve fails to predict the experimental results at the highest velocities. We see in Fig. 16(a) that the theoretical results underestimate the lift amplitude, not following now the same trend with the reduced frequency. The values for the thrust are closer to the analytical prediction, but the experimental trend is quite different than expected. As mentioned above, the dimensionless stiffness becomes too small for this velocity ($S < 1$, see Table III). When the stiffness is so low, both the assumption of small deformation and the approximation of the deformation model lose validity, as more natural modes of chordwise deformation appear,[21] with an undulatory behavior of the wing.[31]

Compared now with the previous results for the wing incorporating carbon fiber rods, we see that the amplitude of the lift oscillations is significantly lower when the wing is more flexible. For the thrust

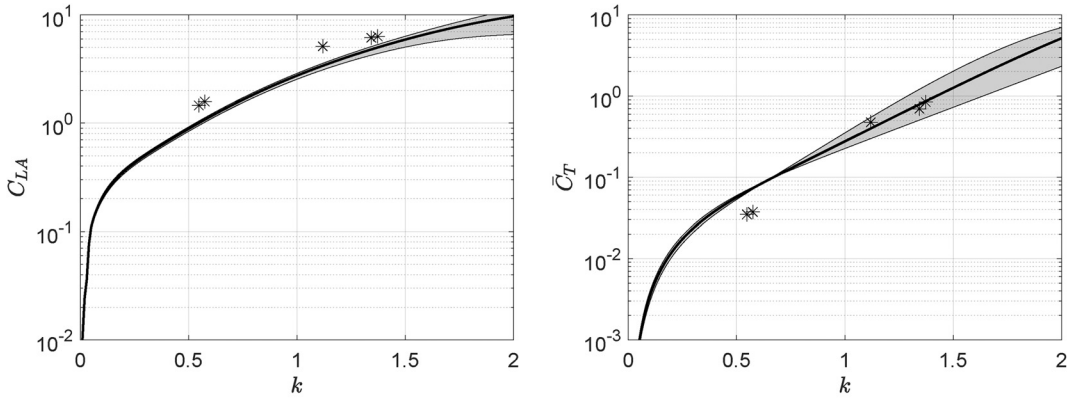

(a) Amplitude of the lift force. (b) Mean thrust coefficient.

FIG. 14. Comparison of the experimental results for the wing with steel rods (stars) and the theoretical curves at the first operating condition of the wind tunnel ($U \approx 2$ m/s). The shaded area represents the uncertainty associated with the velocity ($\pm$ 0.5 m/s).

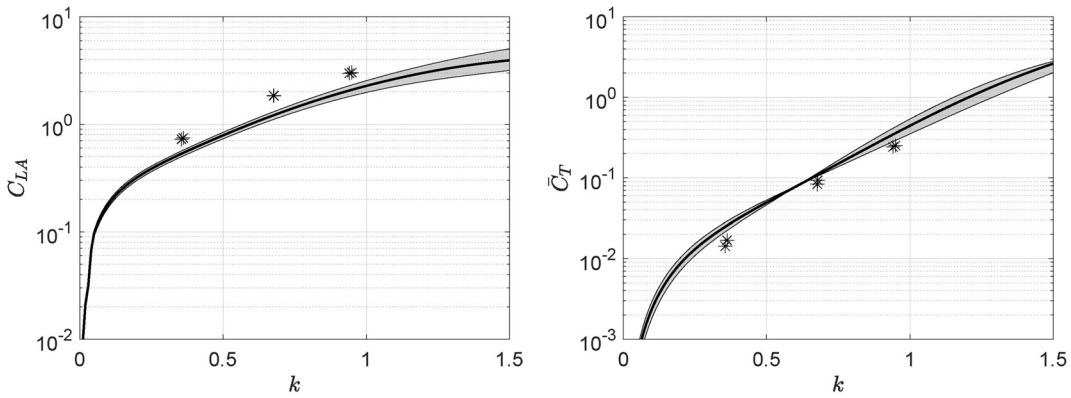

(a) Amplitude of the lift force. (b) Mean thrust coefficient.

FIG. 15. Comparison of the experimental results for the wing with steel rods (stars) and the theoretical curves at the second operating condition of the wind tunnel ($U \approx 3$ m/s). The shaded area represents the uncertainty associated with the velocity ($\pm$ 0.5 m/s).

forces, the behavior depends on the values of the reduced frequency. For values below the critical k, the mean thrust decreases with flexibility. Then, for higher frequencies, the behavior is the opposite and the thrust increases with the flexibility. However, as the frequency increases even further, the slope of the thrust curve starts to reduce. Then, at high frequency and low stiffness, the thrust becomes smaller with a more flexible behavior.

In summary, it is observed that the lift forces are generally underestimated and, therefore, the flexural deformations were higher than expected, causing the results to show a more flexible behavior, leading to an increase in the thrust for the wing with carbon fiber rods and a reduction for the wing with steel rods, in particular at high frequencies and velocities.

VI. CONCLUSION

This work presents an analysis of the forces on a flapping wing, comparing analytical expressions for a flexible heaving foil[21] with wind tunnel force measurements. To go from the 2D formulation to the case of a finite flapping wing, an analogy based on the equivalent stiffness, mass, and amplitude is proposed. The experiments are performed with two wings with the same construction but different chordwise stiffness, to analyze the effects of flexibility on the thrust and lift forces. The wing design is based on the E-Flap ornithopter,[8,33] where the chordwise rods, originally of carbon fiber and 2 mm of diameter, are the structural elements that provide stiffness to the wing surface. An alternative more flexible wing with steel rods of diameter 1 mm is also used. The chordwise resonance frequency is approximated by a theoretical analysis and then validated for the more flexible wing with an experimental testbed designed for this purpose.

The resonance frequency and the wing mass are the only terms of the wing design needed to formulate the analogy, leading to the definition of mass ratio and dimensionless stiffness.[21] The characteristic amplitude is taken at 1/3 of the wingspan from the wingtip. Even though inertial forces do not contribute to the time-averaged forces, they have to be considered for comparison of the temporal evolution of forces, as well as the amplitude of oscillations. However, the

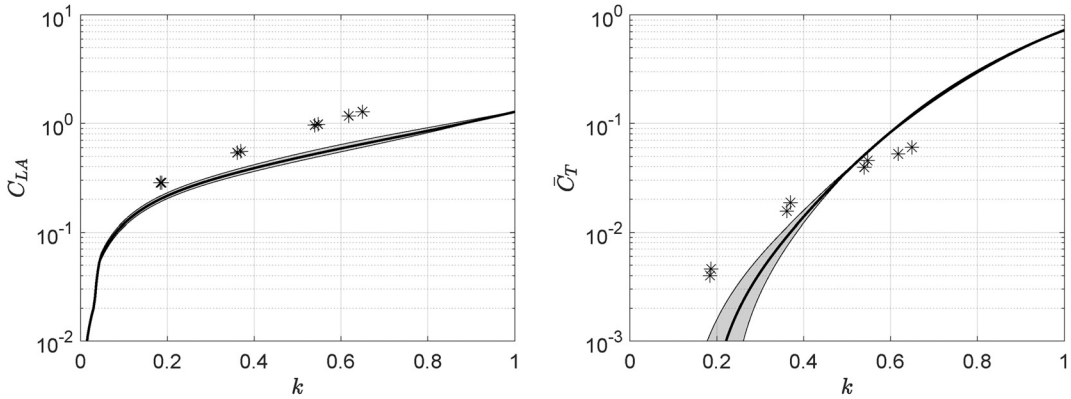

(a) Amplitude of the lift force. (b) Mean thrust coefficient.

FIG. 16. Comparison of the experimental results for the wing with steel rods (stars) and the theoretical curves at the third operating condition of the wind tunnel ($U \approx 6$ m/s). The shaded area represents the uncertainty associated with the velocity ($\pm$ 0.5 m/s).

proposed analogy does not consider the 3D effects on wing deformation or the vorticity of the air flow, since the analysis focuses on estimating the trends and magnitudes of the forces, and not on the accuracy of the results, for which one has to resort to complex numerical simulations or *ad hoc* models based on experimental results.

A comparison of the analogy and the wind tunnel experiments shows good alignment of the theoretical results with the actual measurements for both wings. Although the amplitude of the lift oscillations is slightly underestimated by the theory, possibly because of the large amplitude of the flapping movement, the experimental results showed a trend similar to that predicted by the analytical results. The source of underestimation of the lift oscillations and in the thrust coefficient may be mainly due to the approximation of the flapping amplitude, taken at 1/3 of the wingspan from the wingtip, and to nonlinear effects when the Strouhal number is not small enough. However, other aspects such as 3D flexibility effects and tip vortices would lead to overestimated lift oscillations, as both flexibility and finite wing effects reduce the wing lift. A more detailed analysis of finite wing effects and vorticity distribution for flapping wing is necessary to fully understand the aerodynamic phenomena.

The temporal evolutions along the flapping cycle agree quite well between theoretical and experimental results, and the lift amplitude and the mean thrust are correctly predicted for a wide set of conditions. Specific errors at certain velocities and reduced frequencies cannot be due to general aspects of the experiments, such as the non-ideal sinusoidal input, the manual manufacturing of the wing or the non-continuous wing surface due to the structural elements in the lower surface, as they would affect experiments at different frequencies and velocities. Thus, the theoretical analysis works for all ranges of velocities and flapping frequencies in which the FWAV usually flies, except when the characteristic dimensionless stiffness becomes too small for the theory to be valid (stiffness parameter $S < 1$). For those cases with very small stiffness, analysis considering bat wings are more appropriate.[29]

ACKNOWLEDGMENTS

The authors acknowledge receiving support from the Advanced Grant of the European Research Council GRIFFIN, Action 788247 and the MCIyU/AEI Grant PID2023-150588NB-I00. Ernesto Sanchez-Laulhe acknowledges receiving support through his predoctoral contract at the University of Malaga.

Funding for open access charge: Universidad de Málaga / CBUA.

AUTHOR DECLARATIONS

Conflict of Interest

The authors have no conflicts to disclose.

Author Contributions

Ernesto Sanchez-Laulhe: Conceptualization (equal); Data curation (equal); Formal analysis (lead); Investigation (equal); Methodology (lead); Software (equal); Validation (equal); Visualization (equal); Writing – original draft (equal). **Ramon Fernandez-Feria:** Conceptualization (equal); Formal analysis (supporting); Funding acquisition (equal); Investigation (equal); Methodology (supporting); Resources (equal); Supervision (equal); Writing – review & editing (equal). **Mario Hernandez:** Conceptualization (equal); Methodology (equal); Resources (equal); Validation (equal). **Anibal Ollero:** Conceptualization (equal); Funding acquisition (equal); Project administration (equal); Supervision (equal); Writing – review & editing (equal).

DATA AVAILABILITY

The data that support the findings of this study are available from the corresponding author upon reasonable request.

APPENDIX A: FUNCTIONS OF THE PIVOT POINT AND THRUST TERMS FOR THE ANALOGY OF THE FLAPPING WING

The functions of the pivot point for Eqs. (15) and (16) are the following:

$$s_f(a) = \frac{141 + 168a + 1281a^2 - 1120a^3 + 1015a^4 - 840a^5 + 315a^6}{630(1-a)^2}, \tag{A1}$$

$$A = a^2\left[1 + \frac{2a}{3(1-a)} + \frac{a^2}{6(1-a)^2}\right], \tag{A2}$$

$$B = 2a\left[1 + \frac{a}{1-a} + \frac{a^2}{3(1-a)^2}\right], \tag{A3}$$

$$D = 1 + \frac{2a}{1-a} + \frac{a^2}{(1-a)^2}, \tag{A4}$$

$$E = \frac{2}{3(1-a)}\left(1 + \frac{a}{1-a}\right), \tag{A5}$$

$$J = \frac{1}{6(1-a)^2}, \tag{A6}$$

$$\mathscr{C}(k) = \frac{H_1^{(2)}(k)}{iH_1^{(2)}(k) + H_1^{(2)}(k)} = \mathscr{F}(k) + i\mathscr{G}(k). \tag{A7}$$

The functions of the pivot point for Eqs. (17) and (18) are given by

$$A_{l2} = \frac{13 + 48a^2 - 64a^3 + 24a^4}{48(1-a)^2}, \tag{A8}$$

$$A_{l1} = \frac{3 + 12a - 12a^2 + 4a^3}{6(1-a)^2}, \tag{A9}$$

$$A_{g1} = \frac{15 - 48a + 96a^2 - 80a^3 + 24a^4}{48(1-a)^2}, \tag{A10}$$

$$A_{g0} = \frac{3 - 24a + 24a^2 - 8a^3}{12(1-a)^2}. \tag{A11}$$

The functions for the thrust coefficient in Eq. (19) are

$$t_h = -2\mathscr{G}_1(k), \tag{A12}$$

$$t_{hd} = 4\left(a - \frac{1}{2}\right)\left(\mathscr{G}_1(k) - \frac{\mathscr{F}_1(k)k}{2}\right)\sin(\psi_d) + 4\left[\mathscr{F}_1(k)\left(\frac{1}{2} - a\right) - \mathscr{G}_1(k)k\left(a^2 - \frac{3}{2}a + \frac{3}{4}\right)\right]\cos(\psi_d), \tag{A13}$$

TABLE II. Series of experiments performed with the wing incorporating carbon fiber rods.

n	f (Hz)	U (m/s)	T (^oC)	S	k	St	Re	C_{LA}	$\bar{C}_T$
1	1.10	1.7	27.5	157.8	0.61	0.26	3.2×10^4	1.80	0.059
2	2.34	1.8	27.5	140.8	1.19	0.51	3.4×10^4	7.77	0.361
3	3.45	1.8	27.5	140.8	1.76	0.76	3.4×10^4	15.32	1.454
4	1.11	1.7	27.5	157.8	0.60	0.26	3.2×10^4	2.10	0.058
5	2.30	1.9	27.5	126.3	1.12	0.48	3.6×10^4	6.86	0.293
6	3.40	2.3	27.5	86.2	1.37	0.59	4.3×10^4	9.27	0.845
7	1.03	2.8	27.5	58.2	0.35	0.15	5.2×10^4	0.76	0.027
8	2.25	3.0	27.5	50.7	0.70	0.30	5.6×10^4	2.56	0.109
9	3.34	3.3	27.5	41.9	0.96	0.41	6.1×10^4	4.35	0.342
10	1.03	2.8	19.8	57.1	0.35	0.15	5.4×10^4	0.74	0.030
11	2.28	3.0	19.8	49.7	0.71	0.30	5.9×10^4	2.47	0.098
12	3.34	3.2	19.8	43.7	0.98	0.42	6.2×10^4	4.15	0.329
13	3.75	3.3	19.8	41.1	1.07	0.46	6.4×10^4	4.78	0.428
14	1.02	5.5	28.2	15.1	0.17	0.07	1.0×10^5	0.31	0.005
15	2.33	5.8	28.2	13.6	0.38	0.16	1.1×10^5	0.75	0.022
16	3.33	6.1	28.2	12.3	0.51	0.22	1.1×10^5	1.15	0.056
17	4.01	6.1	28.2	12.3	0.62	0.26	1.1×10^5	1.42	0.090
18	1.10	5.6	19.6	14.3	0.18	0.08	1.1×10^5	0.33	0.003
19	2.28	5.6	19.6	14.3	0.40	0.17	1.1×10^5	0.76	0.021
20	3.49	5.8	19.6	13.3	0.56	0.24	1.1×10^5	1.18	0.074
21	3.91	5.9	19.6	12.9	0.62	0.26	1.2×10^5	1.27	0.092

TABLE III. Series of experiments performed with the wing incorporating steel rods.

n	f (Hz)	U (m/s)	T (^oC)	S	k	St	Re	C_{LA}	$\bar{C}_T$
1	1.11	1.8	20.4	8.13	0.58	0.25	3.2×10^4	1.58	0.037
2	2.42	2.0	20.4	6.46	1.12	0.48	3.4×10^4	5.15	0.478
3	3.27	2.2	20.4	5.33	1.37	0.59	3.4×10^4	6.34	0.845
4	1.05	1.8	20.4	8.27	0.55	0.24	3.2×10^4	1.46	0.035
5	2.42	2.0	20.4	6.46	1.12	0.48	3.6×10^4	5.14	0.475
6	3.22	2.2	20.4	5.26	1.34	0.58	4.3×10^4	6.16	0.697
7	1.06	2.7	20.4	3.56	0.36	0.16	5.2×10^4	0.75	0.017
8	2.13	2.9	20.4	3.08	0.68	0.29	5.6×10^4	1.84	0.093
9	3.17	3.1	20.4	2.71	0.95	0.41	6.1×10^4	3.03	0.252
10	1.04	2.7	20.4	3.52	0.36	0.15	5.4×10^4	0.72	0.014
11	2.10	2.9	20.4	2.89	0.68	0.29	5.9×10^4	1.85	0.083
12	3.16	3.1	20.4	2.69	0.94	0.40	6.2×10^4	2.99	0.242
13	1.10	5.5	20.4	0.87	0.19	0.08	1.0×10^5	0.29	0.005
14	2.23	5.6	20.4	0.83	0.37	0.16	1.1×10^5	0.55	0.019
15	3.30	5.6	20.4	0.83	0.55	0.24	1.1×10^5	0.98	0.046
16	4.02	5.8	20.4	0.79	0.65	0.28	1.1×10^5	1.28	0.060
17	1.08	5.5	20.4	0.87	0.18	0.08	1.1×10^5	0.29	0.004
18	2.18	5.6	20.4	0.83	0.36	0.16	1.1×10^5	0.54	0.016
19	3.26	5.6	20.4	0.83	0.54	0.23	1.1×10^5	0.97	0.040
20	3.92	5.9	20.4	0.75	0.62	0.27	1.2×10^5	1.18	0.053

$$t_d = k(1-a)^2\left\{4\mathscr{F}_1(k)\left(\frac{1}{2}-a\right) - \mathscr{G}_1(k)k[1+2(a-1)a]\right\}. \tag{A14}$$

APPENDIX B: PARAMETERS OF THE WIND TUNNEL EXPERIMENTS

Table II shows the characteristic parameters of the experiments conducted with the wing incorporating carbon fiber rods.

Table III shows the characteristic parameters of the experiments conducted with the wing incorporating steel rods.

REFERENCES

[1]G. de Croon, "Flapping wing drones show off their skills," Sci. Robot. **5**, eabd0233 (2020).
[2]G. A. Folkertsma, W. Straatman, N. Nijenhuis, C. H. Venner, and S. Stramigioli, "Robird: A robotic bird of prey," IEEE Robot. Automat. Mag. **24**, 22–29 (2017).
[3]Z. J. Wang, "Dissecting insect flight," Annu. Rev. Fluid Mech. **37**, 183–210 (2005).
[4]M. F. Platzer, K. D. Jones, J. Young, and J. C. S. Lai, "Flapping wing aerodynamics: Progress and challenges," AIAA J. **46**, 2136–2149 (2008).
[5]W. Shyy, H. Aono, S. K. Chimakurthi, P. Trizila, C.-K. Kang, C. E. Cesnik, and H. Liu, "Recent progress in flapping wing aerodynamics and aeroelasticity," Prog. Aerosp. Sci. **46**, 284–327 (2010).
[6]H. V. Phan, S. Aurecianus, T. Kang, and H. C. Park, "Kubeetle-s: An insect-like, tailless, hover-capable robot that can fly with a low-torque control mechanism," Int. J. Micro Air Vehicles **11**, 1756829319861371 (2019).
[7]Z. Tu, F. Fei, J. Zhang, and X. Deng, "An at-scale tailless flapping-wing hummingbird robot. I. Design, optimization, and experimental validation," IEEE Trans. Rob. **36**, 1511–1525 (2020).
[8]R. Zufferey, J. Tormo-Barbero, M. M. Guzmán, F. J. Maldonado, E. Sanchez-Laulhe, P. Grau, M. Pérez, J. Á. Acosta, and A. Ollero, "Design of the high-payload flapping wing robot e-flap," IEEE Robot. Autom. Lett. **6**, 3097–3104 (2021).
[9]J. Gerdes, A. Holness, A. Perez-Rosado, L. Roberts, A. Greisinger, E. Barnett, J. Kempny, D. Lingam, C.-H. Yeh, H. A. Bruck *et al.*, "Robo raven: A flapping-wing air vehicle with highly compliant and independently controlled wings," Soft Rob. **1**, 275–288 (2014).
[10]T. Theodorsen, "General theory of aerodynamic instability and the mechanism of flutter," Technical Report (NACA, 1935).
[11]T. H. von Karman and W. R. Sears, "Airfoil theory for non-uniform motion," J. Aeronaut. Sci. **5**, 379–390 (1938).
[12]I. E. Garrick, "Propulsion of a flapping and oscillating airfoil," Technical Report (NACA, 1936).
[13]J. C. Wu, "Theory for aerodynamic force and moment in viscous flows," AIAA J. **19**, 432–441 (1981).
[14]R. Fernandez-Feria, "Linearized propulsion theory of flapping airfoils revisited," Phys. Rev. Fluids **1**, 084502 (2016).
[15]C.-K. Kang, H. Aono, C. E. Cesnik, and W. Shyy, "Effects of flexibility on the aerodynamic performance of flapping wings," J. Fluid Mech. **689**, 32–74 (2011).
[16]J. Young, "Numerical simulation of the unsteady aerodynamics of flapping airfoils," Ph.D. thesis (University of New South Wales, Australian Defence Force Academy, School of Aerospace, Civil and Mechanical Engineering, 2005).
[17]S. Heathcote and I. Gursul, "Flexible flapping airfoil propulsion at low Reynolds numbers," AIAA J. **45**, 1066–1079 (2007).
[18]D. Kodali and C.-K. Kang, "An analytical model and scaling of chordwise flexible flapping wings in forward flight," Bioinspir. Biomim. **12**, 016006 (2016).
[19]F. Du and J. Wu, "Analytical results for pitching kinematics and propulsion performance of flexible foil," J. Fluid Mech. **979**, A5 (2024).
[20]J. Alaminos-Quesada and R. Fernandez-Feria, "Propulsion of a foil undergoing a flapping undulatory motion from the impulse theory in the linear potential limit," J. Fluid Mech. **883**, A19 (2020).
[21]R. Fernandez-Feria and J. Alaminos-Quesada, "Analytical results for the propulsion performance of a flexible foil with prescribed pitching and heaving motions and passive small deflection," J. Fluid Mech. **910**, A43 (2021).
[22]Y. Chen, C. Wang, J. Zhao, and S. Wang, "Lift of a bio-inspired flapping wing with a dynamic trailing-edge flap in forward flight," Phys. Fluids **35**, 041709 (2023).
[23]J. D. DeLaurier, "An aerodynamic model for flapping-wing flight," Aeronaut. J. **97**, 125–130 (1993).
[24]D.-K. Kim, J.-S. Lee, J.-Y. Lee, and J.-H. Han, "An aeroelastic analysis of a flexible flapping wing using modified strip theory," in *Active and Passive Smart Structures and Integrated Systems 2008* (International Society for Optics and Photonics, 2008), Vol. 6928, p. 69281O.
[25]M. H. Dickinson, F.-O. Lehmann, and S. P. Sane, "Wing rotation and the aerodynamic basis of insect flight," Science **284**, 1954–1960 (1999).
[26]J. Song, H. Luo, and T. L. Hedrick, "Performance of a quasi-steady model for hovering hummingbirds," Theor. Appl. Mech. Lett. **5**, 50–53 (2015).
[27]B. Parslew and W. J. Crowther, "Simulating avian wingbeat kinematics," J. Biomech. **43**, 3191–3198 (2010).
[28]B. Parslew, "Predicting power-optimal kinematics of avian wings," J. R. Soc. Interface **12**, 20140953 (2015).
[29]X. Fan and K. Breuer, "Low-order modeling of flapping flight with highly articulated, cambered, heavy wings," AIAA J. **60**, 892–901 (2022).
[30]F. Ayancik, Q. Zhong, D. B. Quinn, A. Brandes, H. Bart-Smith, and K. W. Moored, "Scaling laws for the propulsive performance of three-dimensional pitching propulsors," J. Fluid Mech. **871**, 1117–1138 (2019).
[31]A. J. Smits, "Undulatory and oscillatory swimming," J. Fluid Mech. **874**, 1–44 (2019).
[32]Z. J. Wang, J. M. Birch, and M. H. Dickinson, "Unsteady forces and flows in low Reynolds number hovering flight: Two-dimensional computations vs robotic wing experiments," J. Exp. Biol. **207**, 449–460 (2004).
[33]E. Sanchez-Laulhe, R. Fernandez-Feria, and A. Ollero, "Simplified model for forward-flight transitions of a bio-inspired unmanned aerial vehicle," Aerospace **9**, 617 (2022).
[34]R. Fernandez-Feria and J. Alaminos-Quesada, "Energy harvesting and propulsion of pitching airfoils with passive heave and deformation," AIAA J. **60**, 783–797 (2022).
[35]E. Sanmiguel-Rojas and R. Fernández-Feria, "Propulsion enhancement of flexible plunging foils: Comparing linear theory predictions with high-fidelity CFD results," Ocean Eng. **235**, 109331 (2021).
[36]E. Sanmiguel-Rojas, J. Perona, and R. Fernandez-Feria, "Force and torque reactions on a pitching flexible aerofoil," J. Fluid Mech. **961**, A34 (2023).
[37]Y. S. Baik, L. P. Bernal, K. Granlund, and M. V. Ol, "Unsteady force generation and vortex dynamics of pitching and plunging aerofoils," J. Fluid Mech. **709**, 37–68 (2012).
[38]R. Fernandez-Feria and E. Sanmiguel-Rojas, "Comparison of aerodynamic models for two-dimensional pitching foils with experimental data," Phys. Fluids **31**, 057104 (2019).
[39]J. Alaminos-Quesada, "Limit of the two-dimensional linear potential theories on the propulsion of a flapping airfoil in forward flight in terms of the Reynolds and Strouhal number," Phys. Rev. Fluids **6**, 123101 (2021).